

Spiral-driven accretion in protoplanetary discs - II Self-similar solutions

Patrick Hennebelle^{1,2}, Geoffroy Lesur^{3,4}, Sébastien Fromang¹

¹ Laboratoire AIM, Paris-Saclay, CEA/IRFU/SAP - CNRS - Université Paris Diderot, 91191, Gif-sur-Yvette Cedex, France

² LERMA (UMR CNRS 8112), Ecole Normale Supérieure, 75231 Paris Cedex, France

³ Univ. Grenoble Alpes, IPAG, 38000, Grenoble, France

⁴ CNRS, IPAG, F-38000 Grenoble, France

Preprint online version: February 5, 2016

ABSTRACT

Context. Accretion discs are ubiquitous in the universe and it is a crucial issue to understand how angular momentum and mass are being radially transported in these objects.

Aims. Here, we study the role played by non-linear spiral patterns within hydrodynamical and non self-gravitating accretion disc assuming that external disturbances such as infall onto the disc may trigger them.

Methods. To do so, we computed self-similar solutions that describe discs in which a spiral wave propagates. Such solutions present both shocks and critical sonic points that we carefully analyze.

Results. For all allowed temperatures and for several spiral shocks, we calculated the wave structure. In particular we inferred the angle of the spiral pattern, the stress it exerts on the disc as well as the associated flux of mass and angular momentum as a function of temperature. We quantified the rate of angular momentum transport by means of the dimensionless α parameter. For the thickest disc we considered (corresponding to h/r values of about 1/3), we found values of α as high as 0.1, and scaling with the temperature T such that $\alpha \propto T^{3/2} \propto (h/r)^3$. The spiral angle scales with the temperature as $\arctan(r/h)$.

Conclusions. The existence of these solutions suggests that perturbations occurring at disc outer boundaries, such as for example perturbations due to infall motions, can propagate deep inside the disc and therefore should not be ignored, even when considering small radii.

Key words. accretion disc – Instabilities – hydrodynamics

1. Introduction

Accretion discs play a major role in astrophysics as they are ubiquitously observed around stars and black holes. A major question regarding disc evolution is obviously how angular momentum and mass are transported radially in reasonably short times (e.g. Pringle 1981). It is widely admitted that local instabilities such as the magneto-rotational instability (MRI, e.g. Balbus 2003) or the gravitational instability (e.g. Lodato & Rice 2004) are responsible for triggering the transport of momentum and mass. Alternatively, winds emitted by magnetic processes into the disc may carry away angular momentum (Turner et al. 2014). While it is now widely demonstrated that such instabilities and wind launching lead to efficient transport, the conditions under which they operate are still the focus of active research. For example, whether protoplanetary (PP) discs are always sufficiently ionised is still a matter of debate (e.g. Lesur et al. 2014).

The essence of these instabilities is to trigger either non-axisymmetric motions or magnetic field configurations within the discs, which therefore exert a torque on the gas and lead to an outward flux of angular momentum. For simplicity reasons, accretion discs have most of the time been studied in isolation, generally starting with discs at equilibrium. A notable exception concerns many of the studies

that have addressed the question of disc formation in the context of molecular core collapse. In that case, the discs are usually massive and self-gravitating and it is generally admitted that angular momentum can then be transported by gravitational torques or by magnetic braking (e.g. Vorobyov & Basu 2008; Machida et al. 2010; Joos et al. 2012; Li et al. 2013; Vorobyov et al. 2015). The importance of pressure exerted at the accretion shock on the fragmentation of self-gravitating discs within dense cores was also stressed by Hennebelle et al. (2004) in this context (see also Harsono et al. 2011).

The possible specific role that external accretion may have on more evolved accretion discs has received much less attention and only a few studies have investigated in details its impact. This includes in particular the analytical study of Spruit (1987) who computed non-axisymmetric and stationary solutions with shocks (see also Larson 1990; Vishniac & Diamond 1989) and the numerical simulations performed by Sawada et al. (1987); Spruit et al. (1987); Rozyczka & Spruit (1993); Yukawa et al. (1997) who studied the effect of external accretion on mass and angular momentum transport within a disc of mass transferring binary system. In this last case, since accretion is due to the companion of the accreting object, it constitutes an obvious cause for the disc to be maintained in a non-axisymmetric state on long timescales, possibly resulting in a significant

torque within the system. Indeed, these authors found that accretion is a possible powerful source of symmetry breaking and results in an efficient transfer of mass.

In the context of PP discs, the impact of accretion has been suggested by Padoan et al. (2005); Throop & Bally (2008); Klessen & Hennebelle (2010); Padoan et al. (2014), who noted, either by measuring the accretion rate \dot{M}_d onto the disc itself from simulations, or by using analytical arguments, that $\dot{M}_d \propto M_*^2$, where M_* is the mass of the star. This relation is very similar to what can be inferred for the accretion rate \dot{M} onto the young stars themselves (e.g. Muzerolle et al. 2005) and suggests that accretion onto PP discs and accretion onto the star are somehow related. We note that recent results indicate a weaker relationship with $\dot{M}_d \propto M_*^{1.4}$ (Venuti et al. 2014) which therefore may weaken this argument. However, they also find an anti-correlation between the accretion rate and the age of the source which is broadly compatible with the idea that infall onto the disc may trigger accretion since infall is likely to decrease with time as well. Recently, Vorobyov et al. (2015, see also Harsono et al.; Bae et al. 2011) performed a series of 2D simulations of self-gravitating and viscous discs embedded in their parent cores and showed that the infall of material, and particularly its specific angular momentum content, has a drastic impact on their evolution.

In most of these studies, the exact role played by accretion is not straightforward to identify since other processes (such as self-gravity and/or explicit viscosity) are generally considered (e.g. Vorobyov et al. 2015). Also, the accretion fluxes that are considered usually corresponds to rapidly accreting system such as class-0 or class-I embedded protostars. However, investigating the role that accretion exactly has by itself, is important because *i*) it is mandatory to distinguish between the various mechanisms in order to disentangle their contributions, *ii*) there are objects for which the role of other mechanisms remains debated such as for example low mass protoplanetary discs. It is therefore important to quantify the possible effect that external accretion could have onto the disc and in particular whether it could trigger a flux of mass down to the star.

As a first step toward solving that question, we recently performed a series of 2D numerical simulations (Lesur et al. 2015, see also Bae et al. 2015) in order to investigate the transport that is triggered by infalling material within a disc that is both unmagnetized and non self-gravitating. We have found that the infalling flow generates very significant disturbances at the outer edge of the disc: when quantified in terms of the classical α parameter (Eq. 39) and for typical accretion rate of $10^{-7} M_\odot \text{yr}^{-1}$, they lead to $\alpha \sim 10^{-2}$. Moreover, at small radii, the effective α does not go to zero but instead seems to reach a plateau with values of the order of a few times 10^{-4} . These important results therefore open up the possibility that external disturbances can propagate through the disc and generate angular momentum transport even at small radii.

As the physical understanding leading to such a behaviour remains to be clarified, it is useful to study analytical solutions. This is the aim of the present paper where we re-visit, and extend, the self-similar solutions of non-axisymmetric stationary flows studied by Spruit (1987). In these solutions, there is no explicit viscosity and the necessary dissipation is provided by shocks. Such solutions provide a simple framework and give a strong hint about the

physics at play in large scale accretion driven discs. Section two presents the formalism and the method we used to solve the equations. Particular emphasis is made of the nature and the role played by the critical or transonic points present in the flow and which is playing an important role to understand their mathematical nature. In section three we study the physical properties of these solutions as a function of the disc temperature and discuss the implications. The fourth section concludes the paper.

2. Self-similar solutions of externally driven accretion

Following Spruit (1987), we look for self-similar solutions that could describe the mass and angular momentum flux within a disc that would result from a non-axisymmetry induced by an external influence such as non-axisymmetric accretion onto the disc. The existence of these solutions is important to establish since it suggests that spiral modes indeed exist and can propagate from large radii down to small ones. Our solutions, although close to the case investigated by Spruit (1987), are nevertheless different. First of all, Spruit (1987) includes radiation at the surface of the disc (assuming an appropriate spatial dependence for the opacity) while we will restrict the discussion to locally isothermal discs. This is indeed a more realistic approximation for PP discs and one that has been used by many authors in numerical simulations. This particular issue is important since Spruit (1987) found a significant dependence on γ , the adiabatic index, and it is thus important to clarify the effect that the effective equation of state has on the solutions behaviour. In particular in the limit where $\gamma \rightarrow 1$, the spiral angle seems to converge toward a value close to 90 degrees (see Fig. 2 of Spruit (1987)). Since PP discs are typically locally isothermal one wonders whether such a mode could develop and whether it could lead to significant transport. Second, we explicitly give the dependence of various quantities as a function of the gas temperature, while Spruit (1987) focused onto the dependence on γ . Third, we find that there are two (instead of one as found by Spruit 1987) possible choices for the disc surface density radial profiles. While similar in nature, the two family of solutions differ in an important manner, since they respectively correspond to the two limiting cases of vanishing angular momentum flux and vanishing mass flux. Fourth, we clarify the mathematical nature of the solutions and in particular the topology of the critical points, which play a key role for these solutions and is important to solve the equations numerically. Finally, we describe a simple method to obtain these solutions which may serve as reference to compare to simulations and observational results.

2.1. Ordinary equations for self-similar solutions

The equations we solve are the usual fluid equations. Written in Cylindrical geometry, averaged along the z -direction over the disc scale height, h , and assuming stationarity, they write:

$$\left(u_r \partial_r u_r + \frac{u_\phi}{r} \partial_\phi u_r - \frac{u_\phi^2}{r} \right) = -\frac{\partial_r P}{\Sigma} + g_r, \quad (1)$$

$$\left(u_r \partial_r u_\phi + \frac{u_\phi}{r} \partial_\phi u_\phi + \frac{u_r u_\phi}{r} \right) = -\frac{\partial_\phi P}{r \Sigma}, \quad (2)$$

$$\frac{1}{r} \partial_r (r \Sigma u_r) + \frac{1}{r} \partial_\phi (\Sigma u_\phi) = 0, \quad (3)$$

$$g_r = -\frac{GM}{r^2} = -\Omega^2 r, \quad (4)$$

$$h \simeq \frac{C_s}{\Omega}. \quad (5)$$

The disc is assumed to be locally isothermal meaning that $P = C_s(r)^2 \Sigma$, that is to say the sound speed, C_s , and the temperature, T , depend only on the radius, r . Note that P is the vertically averaged pressure and $\Sigma \simeq 2h\rho$ is the column density and ρ is the midplane density. All the other quantities have their usual meaning. Since no explicit dissipation is considered here, the solutions must necessarily entail shocks, which will then lead to finite energy dissipation. Indeed, angular momentum and mass transport, imply such energy dissipation.

To normalise the system, we use similar conventions as Spruit (1987), namely

$$\begin{aligned} r &= r_0 x, \\ u_r &= r_0 \Omega_0 \tilde{u}_r, \\ u_\phi &= r_0 \Omega_0 (x^{-1/2} + \tilde{u}_1), \\ \Sigma &= \Sigma_0 \tilde{\Sigma}, \\ P &= \Sigma_0 r_0^2 \Omega_0^2 \tilde{T} \tilde{\Sigma}, \end{aligned} \quad (6)$$

where r_0 and Σ_0 are arbitrary radius and surface density, $\Omega_0 = (GM/r_0^3)^{1/2}$. In particular, $r_0 \Omega_0 x^{-1/2}$ is simply the Keplerian velocity.

To obtain self-similar solutions, we introduce a new angular variable, $\psi = \phi + \beta(x)$, that is to say the new angular variable shifts with respect to ϕ when r varies and we look for solutions that can be written as $f(x', \psi)$ instead of $f(x, \phi)$. Using the definitions stated by Eqs.(6), Eqs. (1-3) become

$$\begin{aligned} \tilde{u}_r \partial_x \tilde{u}_r + \tilde{u}_r \beta' \partial_\psi \tilde{u}_r + \left(x^{-3/2} + \frac{\tilde{u}_1}{x} \right) \partial_\psi \tilde{u}_r - \frac{\tilde{u}_1^2}{x} - \\ x^{-2} - 2x^{-3/2} \tilde{u}_1 = -\frac{1}{\tilde{\Sigma}} \left(\partial_x (\tilde{T} \tilde{\Sigma}) + \beta' \partial_\psi (\tilde{T} \tilde{\Sigma}) \right) - \frac{1}{x^2}, \end{aligned} \quad (7)$$

$$\begin{aligned} \tilde{u}_r \partial_x \tilde{u}_1 + \beta' \tilde{u}_r \partial_\psi \tilde{u}_1 + \left(\frac{1}{x^{3/2}} + \frac{\tilde{u}_1}{x} \right) \partial_\psi \tilde{u}_1 + \frac{\tilde{u}_r \tilde{u}_1}{x} + \\ \frac{\tilde{u}_r}{2x^{3/2}} = -\frac{1}{x \tilde{\Sigma}} \partial_\psi (\tilde{T} \tilde{\Sigma}), \end{aligned} \quad (8)$$

$$\frac{1}{x} \partial_x (x \tilde{\Sigma} \tilde{u}_r) + \beta' \partial_\psi (\tilde{\Sigma} \tilde{u}_r) + \frac{1}{x} \partial_\psi (\tilde{\Sigma} \tilde{u}_\phi) = 0. \quad (9)$$

Finally, we seek for self-similar solutions in the radius, x and we set

$$\begin{aligned} \tilde{u}_r &= x^{-1/2} U(\psi), \\ \tilde{u}_1 &= x^{-1/2} V(\psi), \\ \tilde{\Sigma} &= x^{-n} R(\psi), \\ \tilde{T} &= x^{-1} T_0, \\ \beta' &= Bx^{-1}. \end{aligned} \quad (10)$$

The parameter B , which is equal to $r \partial_r \psi$ represents the tangent of θ , the angle between the spiral pattern and the radial direction. Plunging these expressions into Eqs. (7-9), we get

$$(BU + 1 + V)U' + BT_0 \frac{R'}{R} \quad (11)$$

$$= (n + 1)T_0 + \frac{1}{2}U^2 + V^2 + 2V,$$

$$(BU + 1 + V)V' + T_0 \frac{R'}{R} = -\frac{1}{2}U(V + 1), \quad (12)$$

$$(-n + \frac{1}{2})RU + (R(BU + 1 + V))' = 0. \quad (13)$$

It is convenient to introduce the variables

$$W = \frac{BU + 1 + V}{\sqrt{1 + B^2}}, \quad (14)$$

which represents the velocity component normal to the spiral pattern and to the shock wave and

$$Z = \frac{U - B(1 + V)}{\sqrt{1 + B^2}}, \quad (15)$$

which represents the velocity component parallel to the shock wave.

With these definitions, Eq. (13) can be rewritten as

$$\frac{R'}{R} = -\frac{W'}{W} + \left(n - \frac{1}{2} \right) \frac{U}{\sqrt{1 + B^2} W}, \quad (16)$$

and easily combines with Eqs. (11-12) leading to

$$\begin{aligned} W' &= \frac{W}{2(1 + B^2)(W^2 - T_0)} \times \\ &\quad (BW^2 + 2BZ^2 - WZ + B(2(n + 1)T_0 - 2) \\ &\quad - T_0(2n - 1) \frac{BW + Z}{W}), \end{aligned} \quad (17)$$

$$\begin{aligned} Z' &= \frac{1}{(1 + B^2)W} \times \\ &\quad (W^2 + \frac{Z^2}{2} - \frac{B}{2}WZ + ((n + 1)T_0 - 1)). \end{aligned} \quad (18)$$

Equations (17-18) are ordinary equations of W and Z . They present a critical point at $W = \sqrt{T_0}$, that is to say when the velocity perpendicular to the spiral pattern is equal to the sound speed. As discussed in the next session, the critical point, which must be crossed smoothly, plays an important role to obtain these solutions.

2.2. Boundary conditions

The boundary conditions are 2π periodic. However, we allow the disc to have several identical spiral arms, so we ask our solutions to be $2\pi/m$ -periodic, where m is the number of spiral arms of the solution.

2.3. Conserved quantities

Conservation of mass and momentum in the disc leads to several constraints that have to be satisfied by the solutions. These constraints are of two types: jump conditions and integral conditions. These two types of conditions express the continuity of mass and momentum fluxes.

2.3.1. Jump conditions

As discussed above, since the solutions ought to describe transport of angular momentum and mass, there is unavoidably energy dissipation in the process. Because the equations do not entail any viscous terms, it implies that shocks must be present. Therefore the present solutions must satisfy Rankine-Hugoniot conditions through the shock that is to say the flux of mass and momentum must be continuous. This leads to

$$R_1 W_1 = R_2 W_2, \quad (19)$$

$$Z_1 = Z_2, \quad (20)$$

$$R_1 W_1^2 + R_1 T_0 = R_2 W_2^2 + R_2 T_0. \quad (21)$$

The last expression can be replaced by the relation

$$W_1 W_2 = T_0, \quad (22)$$

where the subscripts 1 and 2 represent the pre- and post-shock material. To obtain this last relation, we can simply combine Eq. (19) and Eq. (21).

2.3.2. Integral conditions

Our disc model exhibits two important conservation equations, the conservation of mass (Eq. 13) and the conservation of angular momentum

$$\frac{1}{r} \partial_r (r (\Sigma r u_\phi) u_r) + \frac{1}{r} \partial_\phi ((\Sigma r u_\phi) u_\phi) = -\partial_\phi P, \quad (23)$$

which can easily be obtained by combining Eqs. (2-3) and where, as before, stationarity is assumed and integration through the disc is performed. Using the self-similar variables, we get

$$(-n+1)RU(1+V) + (R(1+V) \times (BU+1+V) + T_0 R)' = 0. \quad (24)$$

Integrating Eqns. (13) and (24) between 0 and $2\pi/m$, and making use of the periodic boundary conditions, we obtain the constraints

$$(-n+1/2) \int_0^{2\pi/m} RU d\psi = 0 \quad (25)$$

$$(-n+1) \int_0^{2\pi/m} RU(1+V) d\psi = 0 \quad (26)$$

This implies that either the azimuthally averaged mass flux $\int_0^{2\pi/m} RU d\psi$ or the angular momentum flux $\int_0^{2\pi/m} RU(1+V)$ has to be zero. Although solutions with zero mass and angular momentum flux are *a priori* possible for arbitrary n (but likely do not satisfy Eq. 19), we will focus on more physical solutions: constant mass flux solutions with $n = 1/2$ (which corresponds to the choice made in Spruit 1987) or constant angular momentum flux solutions with $n = 1$. Note that since the temperature is proportional to $1/r$, this implies that the disc thickness, $h \simeq C_s/\Omega \propto r$. Thus the density profile is $\rho \propto r^{-(n+1)} = r^{-3/2}$ for $n = 1/2$ and $\rho \propto r^{-2}$ for $n = 1$.

In the constant mass flux case ($n = 1/2$), we see from Eq. (13) that

$$RW = K, \quad (27)$$

where K is an arbitrary constant. In other words, the density variable R is inversely proportional to the velocity component perpendicular to the shock. This automatically ensures that Eq. (19) is satisfied. Note that since the present solutions are stationary, a mass flux through the disc implies that the central mass increases with time (as will be seen the flux is inwards, as expected).

On the other hand, solutions with $n = 1$ present a flux of angular momentum through the disc but no flux of mass. This implies that while the particle fluids move on closed orbits, angular momentum is transported radially during one cycle. Therefore this implies that a source of angular momentum must be present in the centre. What this source exactly represents physically can be debated. One possibility is that these solutions could represent regimes, limited in time, during which the inner part of the disc is providing the corresponding amount of angular momentum. This is typically what happens in the context of the so-called dead disk as emphasized by Siuniae & Shakura (1977) and D'Angelo & Spruit (2012), which can arise when a central object is magnetically coupled to the disc and exchange angular momentum with it. While generally the solutions are time-dependent, in some circumstance a stationary regime has been inferred. The solutions however make the assumption of an axisymmetric disc and use the α modelling. The present solutions may therefore offer a complementary description in which the mechanisms responsible for the angular momentum transport through the disc is explicitly described. It is also interesting to note that Siuniae & Shakura (1977) predict the column density of the dead disc to have $n = 11/10$ while it has $n = 1$ in our case. Similarly, the steady α disc has $n = 3/4$ while it is $n = 1/2$ for the self-similar non-axisymmetric disc. It is likely the case that for different values of n , the disc is not stationary¹. These solutions would be limited in time since the amount of angular momentum that a star possesses is fairly limited. In this respect, another possible interesting application could be the circumbinary discs (Dubus et al. 2002).

Using Eq. (24) and $n = 1$, we get

$$R = \frac{K}{W(W - BZ) + T_0}. \quad (28)$$

With this expression, it is easy to show that Eq. (19) is automatically satisfied when conditions (20) and (21) are valid. Therefore these solutions are physically meaningful, at least in this respect.

2.4. The critical point

The other constraint comes from the critical point that must be crossed smoothly. Since the existence of shocks connecting supersonic and subsonic regions is necessary, and since the solutions are $2\pi/m$ periodic, there must be a smooth transition between the subsonic and the supersonic

¹ An interesting unsolved question is whether different values of n would correspond to unstationary discs whose average momentum and mass fluxes could be reasonably described by the expression we obtain here. Indeed as shown later the effective α we get does not change much between $n = 1/2$ and $n = 1$ and it is therefore tempting to assume that it could also be the case for n not too different from these 2 values.

regions implying that crossing the critical point is unavoidable. Mathematically, this implies that both the numerator and the denominator of Eq. (17) must vanish at that location, leading to the two conditions

$$W_c = \pm \sqrt{T_0}, \quad (29)$$

$$BW_c^2 + 2BZ_c^2 - W_cZ_c + B(3T_0 - 2) = 0, \quad (30)$$

which gives:

$$Z_c = \frac{1}{2B} \left(n\sqrt{T_0} \pm 2\sqrt{\frac{n^2T_0}{4} + B^2 - 2B^2T_0} \right). \quad (31)$$

This last equation reveals in particular that the condition

$$T_0 < \frac{1}{2} \text{ or } B^2 > \frac{-n^2T_0}{4(1-2T_0)}. \quad (32)$$

must be satisfied for Z_c to be real. Since discs are flat object, $h/r \simeq \sqrt{T_0}$ is expected to be small. Therefore, in practice, this condition does not restrict the values of B and T_0 .

The consequence of the existence of the critical point is that in most of the possible range of parameters, the critical point constitutes a constraint that must be fulfilled, thereby reducing by one the number of degrees of freedom of the system. Note that strictly speaking a careful study of its topology is actually required to understand exactly the constraints it brings to the system (see appendix A).

2.5. Numerical method

The problem we are facing consists in solving the two ordinary equations given by Eqs. (17-18) between 0 and $2\pi/m$. Mathematically, there are thus five independent parameters, the values $W(0)$ and $Z(0)$, as well as B , T_0 and m . On the other hand, there are two constraints coming from the shock conditions and one from the critical point. This implies that there are two free parameters that should be varied. In the following we adopt the temperature, T_0 , and the mode number m as the free parameters and we look for the values of B , $W(0)$ and $Z(0)$ that satisfy the three constraints. Note that there might exist solutions which entail several non-identical shocks and could constitute a broader class of solutions than the periodic solutions considered here.

One difficulty in solving Eqs. (17-18), is to treat the critical point, which as described in the appendix A is a saddle. To solve this system, we first introduce a new variable s as described in the appendix A. The new equations Eqs. (A.1-A.3) do not present any singularity and this is the ones we used to perform the numerical integration using a standard Runge-Kutta integration. For this purpose we first specify a grid of the s variable in decreasing order. To initialise the solution, it is necessary to perform an expansion around the critical point as specified by Eqs. (A.4-A.6), in particular specifying the sign of $d\psi$. The two other quantities δW and δZ are along the eigenvector of the negative eigenvalue. We perform two integrations, one toward the left ($d\psi < 0$) and one toward the right ($d\psi > 0$). We then integrate toward the right (left) until either ψ reach the value $2\pi/m$ ($-2\pi/m$) or reach a stagnation point, i.e. ψ starts decreasing (increasing).

Once this is done, we look for pairs of points, which $i)$ are located at two different sides of the critical point,

$ii)$ satisfy the Rankine-Hugoniot conditions. To do so, we define a norm, \mathcal{N} , given by:

$$\mathcal{N} = \sqrt{\left(\frac{\psi_1 - \psi_2}{\frac{2\pi}{m}} - 1\right)^2 + \left(\frac{Z_1}{Z_2} - 1\right)^2 + \left(\frac{W_1W_2}{W_c^2} - 1\right)^2}, \quad (33)$$

and we then select the pair of points which corresponds to the minimum value. Finally, we iterate on B , the spiral angle, using a simple bisection method, in order to minimise the norm. We use about 250,000 grid points for each of the two trajectories and we require to stop the iterations when B has varied by less than 10^{-5} with respect to the last iteration. We typically obtained a clear minimum of \mathcal{N} with values of the order of 10^{-5} . To demonstrate that convergence has been reached we have also used 50,000 grid points instead. The corresponding norm is, as expected, larger with values of the order of 10^{-4} . The solutions obtained with these two numbers of grid points are nearly indistinguishable apart for one particular quantity that we discuss in section 3.

Finally, to get a fully analytical expression of the solutions, we present in the appendix C an approximated resolution valid at low temperature and high m .

3. Results

3.1. A sample of solutions

Figure 1 shows the $m = 2$ solutions for 15 temperature values equally spaced between 0.18 and 0.012 (the smallest temperatures correspond to the more uniform profiles). The left column corresponds to $n = 1/2$ and the right column to $n = 1$. The red part of the curves corresponds to the subsonic regions while the blue part represents the supersonic part of the flow. The critical point is at the junction of the two. For large temperatures, all fields vary substantially with ψ implying rather dynamical regimes. For example the velocity perpendicular to the spiral pattern, W , becomes up to two times larger than the sound speed while the azimuthal velocity, v , is as small as -0.7 implying that the gas is then rotating at a velocity of about $\simeq 0.3$ times the Keplerian velocity (equal to 1 with these units). At the largest temperature, the density varies by a factor of about 4 while at smaller temperatures ($T_0 \simeq$ a few 0.01), the variations present a much smaller amplitude. Typically, at these low temperatures, the radial velocity, W , varies by about 20% while the azimuthal velocity presents even smaller variations. These solutions therefore describe a flow that is close to rotational equilibrium. Interestingly, the radial velocity, U , changes sign typically around $\psi \simeq 1$. It is always negative in the subsonic region and positive at the end of the supersonic one. This structure is actually necessary to insure an inward (outward) flow of matter (momentum) and a vanishing flow of angular momentum (mass), a point that will be further discussed and quantified in Sect. 3.3. The shape of the two families of solutions ($n = 1/2$ and $n = 1$) remains altogether very similar. As discussed previously and confirmed below, the solutions are however quite different in terms of global mass and angular momentum fluxes.

In Appendix B, we also show the $m = 5$ modes.

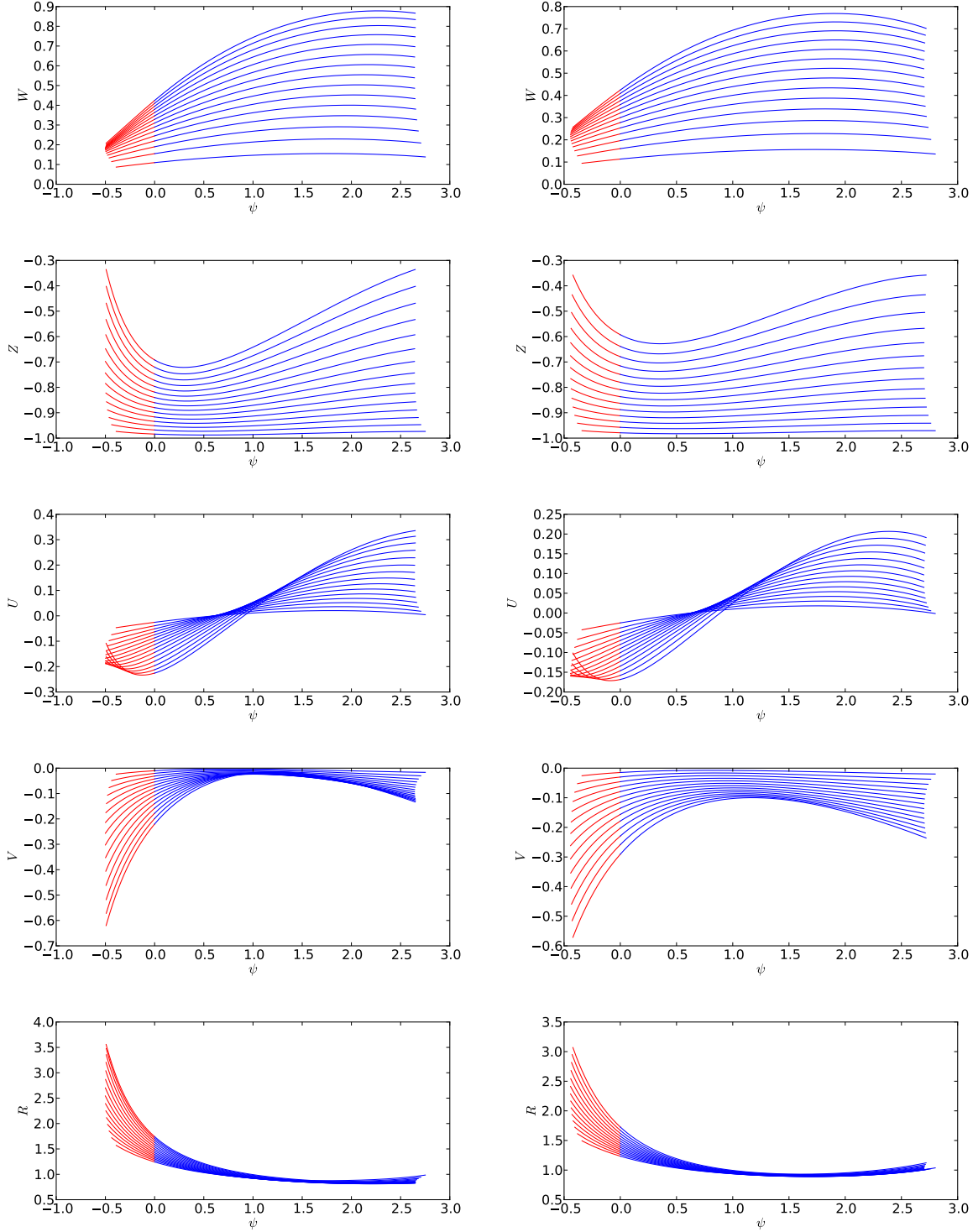


Fig. 1. Mode $m = 2$ for $n = 1/2$ (left) and for $n = 1$ (right). Various fields for a series of temperatures equally spaced between $T_0 = 0.18$ (corresponding to the curves with more pronounced variations) and $T_0 = 0.012$ (corresponding to flatter curves). The red parts of the curve correspond to the subsonic regions and the blue parts to the supersonic ones.

3.2. Dependence of spiral angles on T_0

Figure 2 displays the logarithm of the angle of the spiral pattern, $B = \tan \theta$, as a function of $\log(T_0)$ for the $m = 2-5$ modes. At low temperatures, $T_0 < 0.1$, we find that $B \simeq T_0^{-1/2}$, meaning that the spiral pattern angle is inversely proportional to the local sound speed.

This can be understood easily in the weak shock regime, which is relevant in the limit $T_0 \ll 1$ (thin disc limit). In this limit, the shock front speed is equal to the sound speed C_s and the Keplerian rotation profile is barely perturbed by the presence of a shock. For the spiral shock to be stationary, the Keplerian velocity projected onto the normal to the shock has to be equal to the sound speed

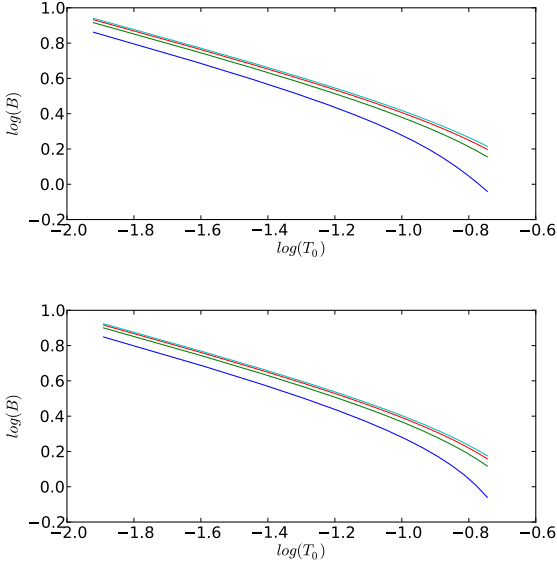


Fig. 2. $B = \tan \theta$, the angle of the spiral pattern as a function of T_0 for the four modes $m = 2, 3, 4, 5$. Top panel is for $n = 1/2$ and bottom one for $n = 1$.

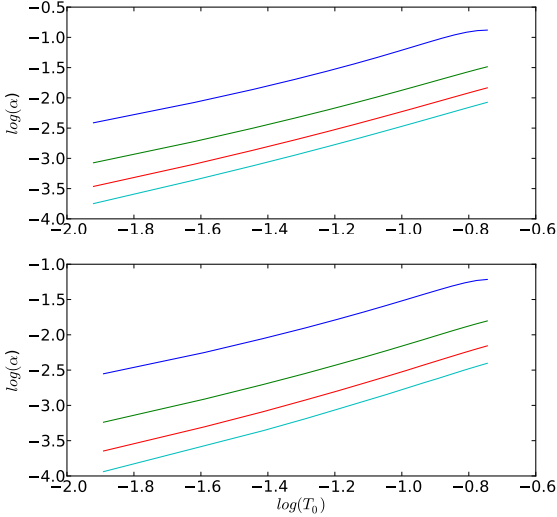


Fig. 3. The α value for $n = 1/2$ (top panel) and $n = 1$ (bottom panel) as a function of T_0 for the four modes $m = 2, 3, 4, 5$.

$C_s(R) \simeq \Omega R \cos(\theta)$, which can be transformed into

$$B \simeq \left(\frac{1 - T_0}{T_0} \right)^{1/2} \quad (34)$$

Stiffer variations are found for higher temperatures where B increases more rapidly with T_0 , as expected from this simple linear analysis. Finally, the angle also slightly increases with the mode number, m .

3.3. Mass flux and stress

3.3.1. Definitions

We now describe and quantify the global mass and momentum fluxes associated with these solutions. More precisely,

we are interested in the flux of mass $\int u_r \Sigma r d\phi$ that we write as

$$\mathcal{F} = \int_0^{2\pi} R(\psi) U(\psi) d\psi, \quad (35)$$

It is known (e.g. Balbus & Papaloizou 1999) that the fluxes of mass and the stress are related to each other through the relation

$$\langle \Sigma u_r \rangle = - \frac{1}{\partial_r (\Omega r^2)_r} \partial_r \langle \Sigma r^2 \delta u_r \delta u_\theta \rangle. \quad (36)$$

In this expression, $\delta u_r = u_r - \langle u_r \rangle$, $\delta u_\theta = u_\theta - \langle u_\theta \rangle$ and Ω is the mean rotation value, $\Omega = \langle u_\theta \rangle / r$. While this relation is a good approximation in the general case (because it neglects a time-dependent term), we stress here that it is an exact relation in the present, stationary case. It must therefore be satisfied and constitutes a test for the accuracy of the numerical solutions.

With the self-similar variables, Eq. (36) becomes

$$\mathcal{F} = \mathcal{S} = - \frac{2(1-n)}{1+\mathcal{V}} \int_0^{2\pi} R(\psi) U(\psi) (V(\psi) - \mathcal{V}) d\psi. \quad (37)$$

where

$$\mathcal{V} = \frac{\int_0^{2\pi} R(\psi) V(\psi) d\psi}{\int_0^{2\pi} R(\psi) d\psi}, \quad (38)$$

is the mean value of V . While for $n = 1/2$ the coefficient $2(1-n)$ is equal to 1, it is equal to 0 for $n = 1$, which indicates that in this latter case the mass flux should be zero as already discussed.

It is usual to define the quantity α as given by

$$\alpha = \frac{\langle \Sigma \delta u_r \delta u_\theta \rangle}{\langle \Sigma C_s^2 \rangle}, \quad (39)$$

which leads to

$$\alpha = \frac{\int_0^{2\pi} R(\psi) U(\psi) (V(\psi) - \mathcal{V}) d\psi}{T_0 \int_0^{2\pi} R(\psi) d\psi}. \quad (40)$$

In this last expression U is used instead of $U - \langle U \rangle$ since $\langle V - \mathcal{V} \rangle = 0$.

Finally, we also compute the flux of angular momentum through the disc, which as discussed before is expected to vanish for $n = 1/2$

$$\mathcal{F}_{mom} = \int_0^{2\pi} R(\psi) U(\psi) (1 + V(\psi)) d\psi. \quad (41)$$

Note that when $n = 1$, since the mass flux vanishes, $\int R(\psi) U(\psi) d\psi = 0$, we have the identity

$$\mathcal{F}_{mom} = \mathcal{F}_{mom, n=1} = \alpha T_0 \int_0^{2\pi} R(\psi) d\psi. \quad (42)$$

Note that this expression is valid only if the flux of mass vanishes.

In the following section, since all quantities depend on α , we restrict our attention to its value.

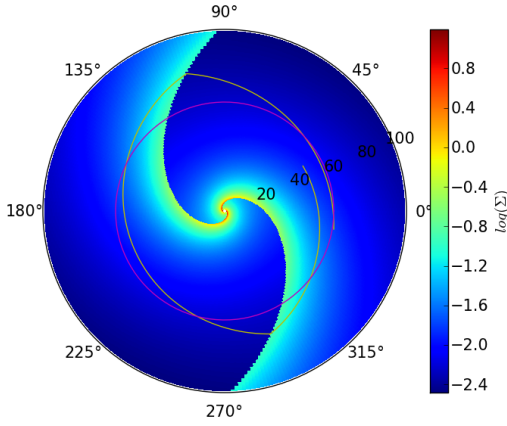


Fig. 4. Case $n = 1/2$. Bidimensional representation of the self-similar spiral pattern for a temperature namely $T_0 = 0.17$ leading to values of $B = \tan \theta$ equal to 1. and to a value of θ equal to about 45 degrees. The yellow line corresponds to the trajectory of a fluid particle and the red circle shows a circular orbit that the same fluid particle would have in a symmetrical disc. Fluid particles are found to spiral inward because of dissipation.

3.3.2. Resulting fluxes: the α value

Top pannel of Fig. 3 displays the values of α as a function of T_0 for the modes $m = 2, 3, 4, 5$. First of all, we see that significant stresses leading to significant mass fluxes are inferred. In terms of the canonical α , values as high as $\simeq 0.1$ are obtained at large temperature. We also find that α scales with temperature roughly as $\alpha \propto T_0^{3/2}$ and decreases as m increases. This is expected since α is proportional to the product of the velocity fluctuations. Indeed, the velocity fields vary over a smaller domain and the typical value of the gradient is obtained at the critical point and does not vary significantly with m (since it depends only on B which does not vary strongly with m). Physically, higher m modes tends to be closer to an axisymmetric configuration.

Note that we have verified that the flux of mass obtained from expression \mathcal{F} and \mathcal{S} are very close to each other. There are however not identical because of the numerical integration. In particular, the flux of mass calculated using expression \mathcal{F} appears to be more noisy. This is because U changes sign and the integral values of the regions where it is either positive or negative are very close. On the other hand, when α is evaluated, $V - \mathcal{V}$ is also changing sign at the same locations as U (reflecting the fact that the radial and azimuthal velocity components are highly correlated) and therefore the sign of the integrand is generally positive, making it less sensitive to the fluctuations.

We have also verified that as expected, the flux of angular momentum is extremely small and indeed equal to zero within the accuracy of the calculation (not displayed here for conciseness).

Figure 3 also shows (bottom panel) α for $n = 1$ as a function of T_0 . The value of α remains quite similar to the case $n = 1/2$ although a little lower (by typically about 20%). This confirms that the influence of the density profile onto the various fields is not too drastic. The fluxes are

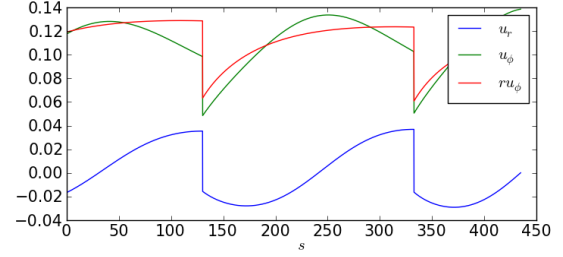


Fig. 5. Radial and azimuthal velocities and angular momentum of the fluid particles along the trajectories displayed in Fig. 4 corresponding to a radius of $r \simeq 60$ for $n = 1/2$.

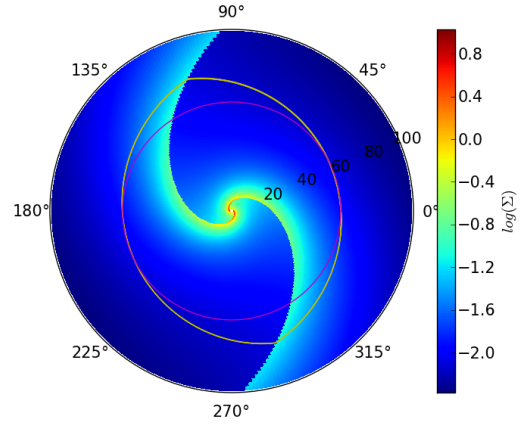


Fig. 6. Case $n = 1$. Bidimensional representation of the self-similar spiral pattern for $T_0 = 0.17$, leading to values of $B = \tan \theta$ equal to $\simeq 1.0$ and θ equal to about 45 degrees. The yellow line corresponds to the trajectory of a fluid particle and the red circle shows a circular orbit that the same fluid particle would have in a symmetrical disc. The trajectory of the fluid particle shows that while the fluid particle has a non circular orbit, it is nevertheless closed. This is because the mass flux vanishes. There is however an outwards flux of angular momentum.

however, as already discussed, quite different. The mass flux is equal to zero within numerical precision (not displayed here for conciseness), while the momentum flux is a simple power law of the temperature, $\simeq T_0^{-2.5}$ similar to the dependence of the mass flux when $n = 1/2$.

3.4. Lagrangian analysis

In order to gain physical insight, it is interesting to follow the trajectory of a fluid particle, that is to say a particle that follows the stream lines. Figure 4 displays a bidimensional view of the density field for a temperature $T_0 = 0.17$ corresponding to the angle $\theta = 45$ degrees. The yellow curves show the trajectory of a fluid particle. It was

obtained by simply solving the two equations

$$\frac{dx}{dt} = v_x, \quad (43)$$

$$\frac{dy}{dt} = v_y. \quad (44)$$

A circle representing the trajectory that would be followed by a fluid particle in a symmetrical unperturbed disc is also plotted for comparison. Because of the self-similar nature of the solutions, we stress that all trajectories are identical to the one displayed there once rescaled and rotated.

As can be seen on figure 4, when the fluid particle encounters the shock, it is deflected inwards (since the velocity, v_\perp decreases while v_\parallel is unchanged). Consequently, it tends to fall toward the disc center. However, as is clear from Fig. 4, there is a density and therefore a pressure gradient, due to the spiral structure, that is pushing the fluid particle outwards. Therefore the fluid particle is decelerated in the radial direction and accelerated in the azimuthal direction. This is even clearer in Fig. 5 in which the radial and azimuthal velocity along with the angular momentum are displayed along the fluid particle trajectory as a function of the curvilinear abscissa s : u_r increases continuously after the shock up to the next shock (with a short phase during which it further decreases for the largest T_0). Similarly, u_ϕ increases continuously between $s = 30$ and $s = 130$ and then decreases. This last phase is simply due to the fact that since the fluid particle is moving outwards, its Keplerian velocity decreases. The evolution of the specific angular momentum is also enlightening. After a steep decrease through the shock, it increases continuously and tends toward a constant value. The physical picture is thus that at the shock, the fluid particle is suddenly slowed down and this results in an exchange of angular momentum, through the pressure forces with the post shock gas. After this point, the particle's momentum increases because of the pressure gradient. Thus the fluid particle is being given angular momentum from the gas that is located at smaller radii. This momentum is then carried along up to the next shock when it will be delivered to higher radii material.

Although the radii of the fluid particle varies non-monotonically during one cycle (i.e. during 2 shocks), it is globally decreasing with time and the particles spiral inwards as expected (the mass flux being negative in that case).

By comparison, Fig. 6 shows the density profile and fluid particle trajectory for $n = 1$ and $B \simeq 1$ (similar to the first panel of Fig. 4). As expected, the orbit (yellow curve) is closed even though it is not circular.

4. Conclusion

We have investigated self-similar solutions of a spiral pattern within a disc. They are similar to the one studied by Spruit (1987) but a different assumption is made regarding the temperature distribution. In addition, different density profiles are considered. These solutions, which are self-similar in radius, depends on the azimuthal angle, and describe a non-linear spiral wave propagating in a centrifugally supported and locally isothermal disc. They feature shocks at which location dissipation takes place. Because the flow is supersonic when the gas enters the shock and subsonic as it emerges, the solutions present a critical sonic

point, which describes the transition from subsonic to supersonic motions. Since the equations have eventually to be solved numerically, we have carefully studied the nature of this critical point and have shown that almost everywhere it is a saddle rather than a node.

Numerically solving the ordinary equations under the constraint that the flow must satisfy the Rankine-Hugoniot conditions through the shock, we obtained a series of profiles for various temperatures and mode number m . We inferred the values of α and showed that it can be as large as ~ 0.1 for the thickest discs for which solutions exist ($h/r \simeq 1/3$). For smaller temperatures, it then drops as $T^{1.5}$ or equivalently as $(h/r)^3$. We found that the spiral angle, θ , increases when T diminishes roughly as $\theta = \arctan(r/h)$. Two density profiles are being explored. For the first one ($n = 1/2$), we find a non-vanishing mass flux and a zero angular momentum flux. For the second one ($n = 1$), the first vanishes but not the latter. The parameter α is however very similar for these two cases, with the steeper profile presenting slightly lower values.

From a Lagrangian analysis of the solutions, it is concluded that in the $n = 1/2$ case the fluid particles spiral inwards and undergo a series of shocks, followed by a pressure acceleration due to the global spiral pattern. During these two phases the fluid particles are respectively losing and gaining angular momentum due to momentum exchange with the surrounding gas. This leads to an inward flux of mass through the disc. In the $n = 1$ case, the fluid particles follow a non-circular closed orbit. There is however an outward flux of angular momentum. While these two types of solutions present different behaviours in terms of fluxes, they are rather similar and typically differ by only a few tens of percents. Their Lagrangian behaviours are also very similar.

Although restricted to particular temperature and density profiles, the existence of these solutions suggests that external perturbations exerted onto accretion discs can propagate deep into the discs and therefore should not be ignored. In many systems, the most natural source of external perturbations is the accretion of external gas which produce shocks at the disc surface.

ACKNOWLEDGMENTS

We thank the anonymous referee for a constructive and helpful report. This research has received funding from the European Research Council under the European Community's Seventh Framework Programme (FP7/2007-2013 Grant Agreement no. 306483).

Appendix A: Topology of the critical points

The topological nature of the critical point is worth studying as it also constraints the values of T_0 and B . In particular, it is important to know whether it is a node or a saddle. In the first case, a one dimensional ensemble of trajectories will be able to cross it while in the second case, only a discrete set of trajectories will have to be considered. To achieve this we introduce a new variable, s , such that

$$\frac{d\psi}{ds} = T_0 - W^2, \quad (\text{A.1})$$

$$\frac{dW}{ds} = -\frac{W}{2(1+B^2)} \times \left(BW^2 + 2BZ^2 - WZ + B(2(n+1)T_0 - 2) - T_0(2n-1)\frac{BW+Z}{W} \right), \quad (\text{A.2})$$

$$\frac{dZ}{ds} = \frac{T_0 - W^2}{(1+B^2)W} \times \left(W^2 + \frac{Z^2}{2} - \frac{B}{2}WZ + ((n+1)T_0 - 1) \right). \quad (\text{A.3})$$

Note that it is also possible to consider $-s$ instead of s , however this leads to unphysical solutions that entail a rarefaction shock, i.e. the gas enters the shock subsonically and leaves it supersonically.

To study the topology of the critical point, we make an expansion in its neighbourhood and obtain a linear system

$$\frac{d\delta\psi}{ds} = -2W_c\delta W, \quad (\text{A.4})$$

$$\frac{d\delta W}{ds} = M_{WW}\delta W + M_{WZ}\delta Z = \quad (\text{A.5})$$

$$\frac{-W_c}{2(1+B^2)} \times \left(\left(2BW_c - Z_c + T_0(2n-1)\frac{Z_c}{W_c^2} \right) \delta W + \left(4BZ_c - W_c - T_0(2n-1)\frac{1}{W_c} \right) \delta Z \right),$$

$$\frac{d\delta Z}{ds} = M_{ZW}\delta W = \quad (\text{A.6})$$

$$\frac{-2\delta W}{(1+B^2)} \times \left(W_c^2 + \frac{Z_c^2}{2} - \frac{B}{2}W_cZ_c + ((n+1)T_0 - 1) \right).$$

The matrix of this linear system admits three eigenvalues, 0, and

$$\lambda_{\pm} = \frac{1}{2} \left(M_{WW} \pm \sqrt{M_{WW}^2 + 4M_{WZ}M_{ZW}} \right). \quad (\text{A.7})$$

Let Y_i^0 be the three eigenvectors associated to the three eigenvalues. In the neighborhood of the critical point, the solutions of the linear system Eqs. (A.4-A.6) are linear combination of Y_i^0 and can be written as

$$Y(s) = \sum_{i=1,3} \alpha_i \exp(\lambda_i s) Y_i^0, \quad (\text{A.8})$$

where α_i are real coefficients. Obviously, if $\lambda_i > 0$, $Y(s) \rightarrow \infty$ implying that α_i must be 0 in order for the corresponding solution to cross the critical point. It is therefore important to know the sign of λ_+ and λ_- . Another possibility is that λ_+ and λ_- are complex conjugate. In this case, the solutions approach the critical point with an oscillating behaviour. Such solutions are not physical either since they imply multi-valuate physical variables at the same location ψ . It is therefore important to study the signs of M_{WW} , M_{WZ} , M_{ZW} and $M_{WW}^2 + 4M_{WZ}M_{ZW}$. Plugging the expression of W_c and Z_c (selecting the “-” sign in Eq. 31), we obtain their values. It is easy to verify that $M_{WW} < 0$ while $M_{WZ} > 0$.

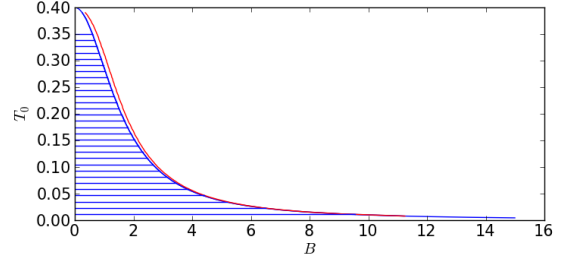


Fig. A.1. Topology of the critical points for $n = 1/2$. Blue: points satisfying $M_{ZW} = 0$. This represents the transition from saddle to node critical points (one negative and one positive eigenvalues). Red: points satisfying $M_{WW}^2 + 4M_{WZ}M_{ZW}$. Transition between the node critical points to oscillatory critical points (two complex conjugate eigenvalues). The physical solutions are to be searched in the dashed area.

The sign of M_{ZW} and $M_{WW}^2 + 4M_{WZ}M_{ZW}$ is less straightforward and we have studied their values numerically (the sign of M_{ZW} can be obtained through a second order polynomial). Figure A.1 shows the curves in the $B - T_0$ plane, which correspond to $M_{ZW} = 0$ (blue curve) and $M_{WW}^2 + 4M_{WZ}M_{ZW} = 0$ (red curve). The possible solutions are located in the dashed region where there is one negative eigenvalue. In this region the critical points are saddle. Strictly speaking, it is also possible to have solutions with critical points located in between the blue and the red curves where the eigenvalues are both negative and the critical points are nodes. These solution however would present a weak discontinuity, that is to say the derivatives of the fluid variables (density and velocity) are discontinuous.

Appendix B: The $m = 5$ mode

For completeness Fig. B.1 shows the $m = 5$ solutions for the same temperatures as in Fig. 1. Altogether, the solutions have similar shape as the $m = 2$ mode but present less variations, therefore as will be seen in Sect. 3.3, they lead to smaller mass fluxes than the $m = 2$ mode.

Appendix C: Analytical expansion in the low temperature limit

Here we present an analytic expansion of Eqs. (17-18) that is valid in the low temperature limit. Since we solved these equations numerically, the aim is more to make the various dependence more explicit rather than obtaining accurate expressions. The approximated expressions are typically good at low temperature and at large m .

Let us expand the perpendicular and parallel velocity, W and Z as

$$\begin{aligned} W(\psi) &= \sqrt{T_0}(1 + w(\psi)), \\ Z(\psi) &= Z_c + z(\psi), \end{aligned} \quad (\text{C.1})$$

where we will assume that $w \ll 1$ and $z \ll Z_c$. Since at the critical point $w = 0$ and $z = 0$, this assumption is clearly verified in the vicinity of the critical point and therefore particularly in the limit of large m . Moreover as discussed previously the spiral parameter, $B = \tan(\theta)$, is

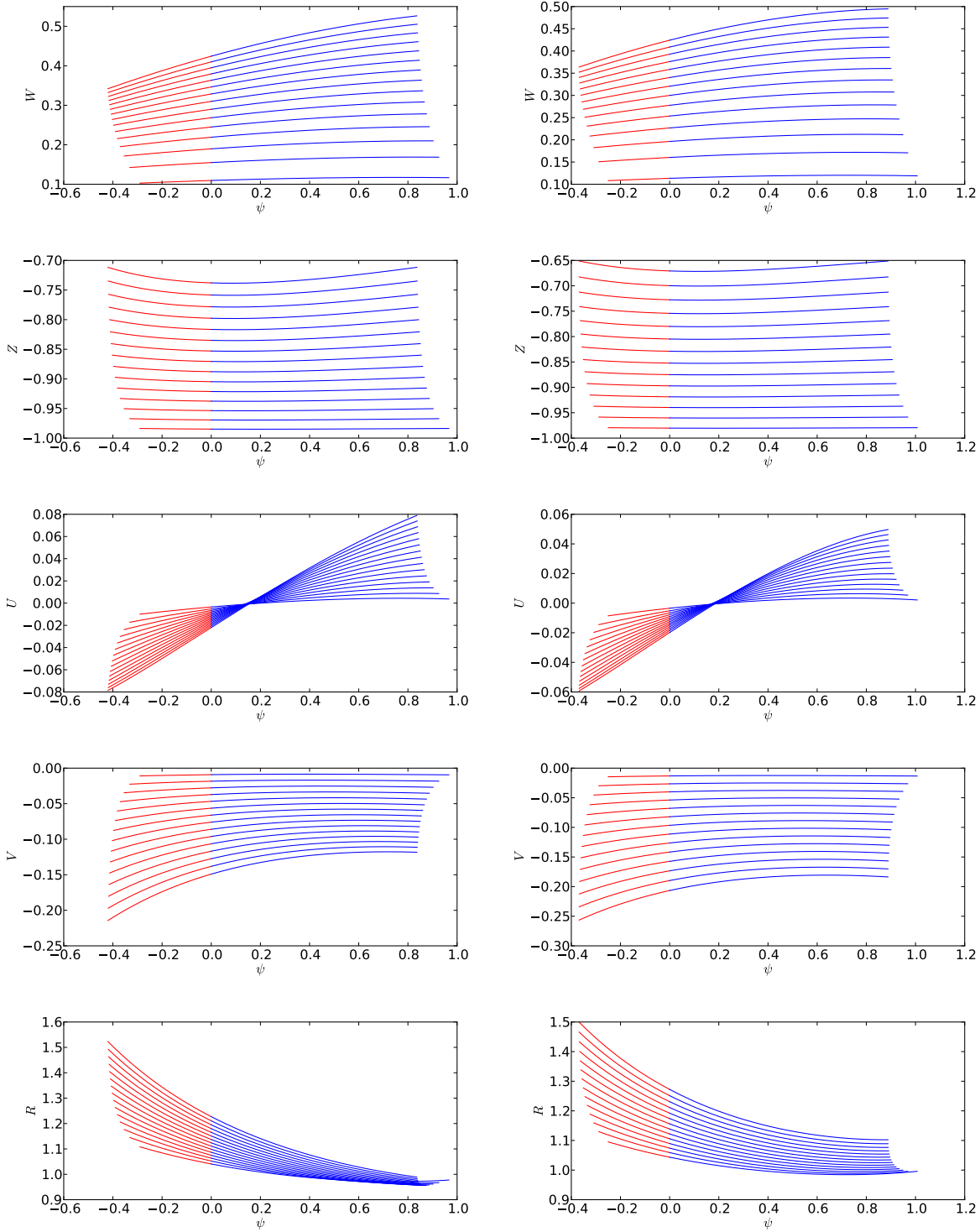


Fig. B.1. Same as Fig. 1 for the modes $m = 5$.

on the order of $1/\sqrt{T_0}$. Thus we write $B = b/\sqrt{T_0}$. Finally, we restrict the calculation to the case $n = 1/2$.

Plugging these expressions into Eqs. (17-18), we get

$$\begin{aligned}
 ww' &= A_1 w + A_2 z, \\
 z' &= B_0 + B_1 w + B_2 z, \\
 A_1 &= \frac{1}{4(T_0 + b^2)} \left((2b - Z_c) \sqrt{T_0} \right) \simeq \frac{3\sqrt{T_0}}{4}, \\
 A_2 &= \frac{1}{4(T_0 + b^2)} \left(\frac{4Z_c}{\sqrt{T_0}} - \sqrt{T_0} \right) \simeq \frac{-1}{\sqrt{T_0}}, \\
 B_0 &= \frac{\sqrt{T_0}}{(T_0 + b^2)} \left(\frac{Z_c^2}{2} - \frac{bZ_c}{2} - 1 + \frac{5}{2}T_0 \right) \simeq (b-1)\sqrt{T_0}, \\
 B_1 &= \frac{\sqrt{T_0}}{(T_0 + b^2)} \left(2\sqrt{T_0} - \frac{b}{2}Z_c \right) \simeq \frac{\sqrt{T_0}}{2}, \\
 B_2 &= \frac{\sqrt{T_0}}{(T_0 + b^2)} \left(Z_c - \frac{b}{2} \right) \simeq \frac{-3\sqrt{T_0}}{2},
 \end{aligned} \tag{C.2}$$

where to get the simplified expressions, we have used that in the limit of low T_0

$$Z_c = -1 + T_0 \frac{1+4b}{4b} \simeq -1, \quad (\text{C.3})$$

while

$$b \simeq 1. \quad (\text{C.4})$$

To get an approximation of Eqs. (C.2) we expand w and z to the second order in $\psi - \psi_c$,

$$\begin{aligned} w(\psi) &= a_1(\psi - \psi_c) + a_2(\psi - \psi_c)^2, \\ z(\psi) &= b_1(\psi - \psi_c) + b_2(\psi - \psi_c)^2, \end{aligned}$$

The coefficients $a_{1,2}$ and $b_{1,2}$ are solutions of the following equations

$$\begin{aligned} a_1^2 &= A_1 a_1 + A_2 b_1, \\ 3a_1 a_2 &= A_1 a_2 + A_2 b_2, \\ b_1 &= B_0, \\ 2b_2 &= B_1 a_1 + B_2 b_1. \end{aligned} \quad (\text{C.5})$$

which leads to

$$a_1 = \frac{1}{2} \left(A_1 + \sqrt{A_1^2 + 4A_2 B_0} \right) \simeq \sqrt{1-b}, \quad (\text{C.6})$$

$$a_2 = \frac{b_2 A_2}{3a_1 - A_1} \simeq -\frac{1}{12} \frac{1}{1 - \frac{1}{4} \sqrt{\frac{T_0}{1-b}}},$$

$$b_1 = B_0 \simeq -\sqrt{T_0}(1-b),$$

$$b_2 = \frac{1}{2}(a_1 B_1 + B_2 B_0) \simeq \frac{1}{4} \sqrt{T_0} \sqrt{1-b}, \quad (\text{C.7})$$

At this stage we have two free parameters, ψ_c and b . They are determined by the two boundary conditions as given by Eqs. (20-22), which in the limit $w \ll 1$ leads to

$$\begin{aligned} w\left(\frac{\pi}{m} - \psi_c\right) &= -w\left(-\frac{\pi}{m} - \psi_c\right), \\ z\left(\frac{\pi}{m} - \psi_c\right) &= z\left(-\frac{\pi}{m} - \psi_c\right). \end{aligned} \quad (\text{C.8})$$

Combining them with Eqs. (C.7), we obtain

$$\begin{aligned} \psi_c &= \frac{b_1}{2b_2} \simeq -2\sqrt{1-b}, \\ a_1 \psi_c &= a_2 \left(\left(\frac{\pi}{m}\right)^2 + \psi_c^2 \right). \end{aligned} \quad (\text{C.9})$$

Combining these two last equations, we get a non-linear equation of b , which can be easily solved using a standard root finder. Once we get b , all quantities are known. A comparison between the numerical solutions and the approximated ones is displayed in Fig. C.1.

References

Bae, J., Hartmann, L., & Zhu, Z. 2015, ArXiv e-prints
 Balbus, S. A. 2003, ARA&A, 41, 555
 Balbus, S. A. & Papaloizou, J. C. B. 1999, ApJ, 521, 650
 D'Angelo, C. R. & Spruit, H. C. 2012, MNRAS, 420, 416
 Dubus, G., Taam, R. E., & Spruit, H. C. 2002, ApJ, 569, 395
 Harsono, D., Alexander, R. D., & Levin, Y. 2011, MNRAS, 413, 423
 Hennebelle, P., Whitworth, A. P., Cha, S.-H., & Goodwin, S. P. 2004, MNRAS, 348, 687

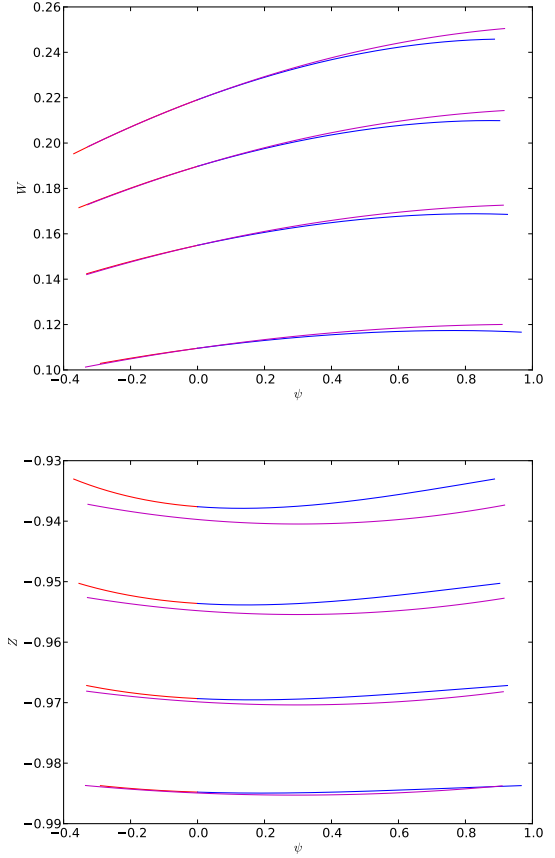


Fig. C.1. Comparison between the numerical solutions (red and blue curves) obtained numerically and the approximated ones presented in this appendix (magenta curves) for $m = 5$ and $T_0 = 0.048, 0.036, 0.024$ and 0.012 . As can be seen they are quite close demonstrating the validity of the approximation.

Joos, M., Hennebelle, P., & Ciardi, A. 2012, A&A, 543, A128
 Klessen, R. S. & Hennebelle, P. 2010, A&A, 520, A17
 Larson, R. B. 1990, MNRAS, 243, 588
 Lesur, G., Hennebelle, P., & Fromang, S. 2015, ArXiv e-prints
 Lesur, G., Kunz, M. W., & Fromang, S. 2014, A&A, 566, A56
 Li, Z.-Y., Krasnopolsky, R., & Shang, H. 2013, ApJ, 774, 82
 Lodato, G. & Rice, W. K. M. 2004, MNRAS, 351, 630
 Machida, M. N., Inutsuka, S.-i., & Matsumoto, T. 2010, ApJ, 724, 1006
 Muzerolle, J., Luhman, K. L., Briceño, C., Hartmann, L., & Calvet, N. 2005, ApJ, 625, 906
 Padoan, P., Haugbølle, T., & Nordlund, Å. 2014, ApJ, 797, 32
 Padoan, P., Kritsuk, A., Norman, M. L., & Nordlund, Å. 2005, ApJ, 622, L61
 Pringle, J. E. 1981, ARA&A, 19, 137
 Rozyczka, M. & Spruit, H. C. 1993, ApJ, 417, 677
 Sawada, K., Matsuda, T., Inoue, M., & Hachisu, I. 1987, MNRAS, 224, 307
 Siunjaev, R. A. & Shakura, N. I. 1977, Pisma v Astronomicheskii Zhurnal, 3, 262
 Spruit, H. C. 1987, A&A, 184, 173
 Spruit, H. C., Matsuda, T., Inoue, M., & Sawada, K. 1987, MNRAS, 229, 517
 Throop, H. B. & Bally, J. 2008, AJ, 135, 2380
 Turner, N. J., Fromang, S., Gammie, C., et al. 2014, Protostars and Planets VI, 411
 Venuti, L., Bouvier, J., Flaccomio, E., et al. 2014, A&A, 570, A82
 Vishniac, E. T. & Diamond, P. 1989, ApJ, 347, 435
 Vorobyov, E. I. & Basu, S. 2008, ApJ, 676, L139
 Vorobyov, E. I., Lin, D. N. C., & Guedel, M. 2015, A&A, 573, A5

Yukawa, H., Boffin, H. M. J., & Matsuda, T. 1997, MNRAS, 292, 321